Multicommodity routing optimization for engineering networks

Alessandro Lonardi,[1,*] Mario Putti,[2] and Caterina De Bacco[1,†]

[1] *Max Planck Institute for Intelligent Systems, Cyber Valley, Tübingen 72076, Germany*

[2] *Department of Mathematics "Tullio Levi-Civita", University of Padua, Via Trieste 63, Padua, Italy*

Optimizing passengers routes is crucial to design efficient transportation networks. Recent results show that optimal transport provides an efficient alternative to standard optimization methods. However, it is not yet clear if this formalism has empirical validity on engineering networks. We address this issue by considering different response functions—quantities determining the interaction between passengers—in the dynamics implementing the optimal transport formulation. Particularly, we compare a theoretically-grounded response function with one that is intuitive for settings involving transportation of passengers, albeit lacking theoretical justifications. We investigate these two modeling choices on the Paris metro and analyze how they reflect on passengers' fluxes. We measure the extent of traffic bottlenecks and infrastructure resilience to node removal, showing that the two settings are equivalent in the congested transport regime, but different in the branched one. In the latter, the two formulations differ on how fluxes are distributed, with one function favoring routes consolidation, thus potentially being prone to generate traffic overload. Additionally, we compare our method to Dijkstra's algorithm to show its capacity to efficiently recover shortest-path-like graphs. Finally, we observe that optimal transport networks lie in the Pareto front drawn by the energy dissipated by passengers, and the cost to build the infrastructure.

I. INTRODUCTION

Finding optimal flow configurations in transport networks is an important problem in many real-world applications. While natural systems like river basins [1–5], leaf venations [6–9], or slime molds [10–17] involve transport of one type of mass only, e.g. water, this may not be the case in several engineering systems. For instance, routing data packets in communication networks, or passengers in urban transportation networks, requires multicommodity approaches where mass of different types interacts in a shared infrastructure, contributing to minimize a unique cost function.

Despite their practical significance, multicommodity algorithms based on optimization routines are burdened by high computational complexity, caused by the simultaneous assignment of multiple commodities. Therefore, practitioners often rely on heuristics and approximations that lead to suboptimal solutions [18]. Distributed approaches like message-passing algorithms have demonstrated encouraging results [19–24], but remain computationally costly in scenarios where there is a large number of origin-destination pairs to be routed, or when the network is not sparse.

A promising approach is that of optimal transport theory. Recent studies [25, 26] have shown that this theoretical formalism can be adapted to address multicommodity scenarios, generalizing well-established results for unicommodity models [27–33]. The works of Lonardi *et al.* [25] and Bonifaci *et al.* [26] focus on a theoretical characterization of the problem, drawing a formal connection between optimal transport and an equivalent dynamical system that is formulated in terms of physical quantities like conductivities and fluxes. They provide theoretical guarantees that are valid for a particular choice of the transport cost function. While preliminary results on multilayer transportation networks [34] suggest an empirical validity of this choice, questions remain open about its applicability in settings involving the transport of passengers.

In this work, we address this concern by studying the behavior of optimal transport approaches for multicommodity routing on urban transportation networks, with an empirical example analysis on the Paris metro network. Our goal is to evaluate how different choices of cost functions impact the resulting distribution of passengers flows. In detail, we search for stationary solutions of a dynamics where edge capacities—conductivities—grow as an increasing function of the total amount of passengers traveling on the edges. We numerically investigate two practical cases, where the dependence between conductivities and fluxes is either with the sum of the passengers traveling through the network (its 1-norm), or with the sum of their squares (its 2-norm). The first choice is more intuitive, since counting the total number of users in a network is a natural metric to evaluate its occupancy. However, the second one provides strong theoretical guarantees in terms of optimal transport theory [25, 26].

We design several experiments to investigate the main properties of optimal network configurations resulting in the two cases. First, we assess the major differences, observing that the 2-norm case tends to dilute more substantially passengers on the network, avoiding heavily trafficked routes. Second, we compare our model with Dijkstra's algorithm [35], a popular approach for shortest-path minimization. We find that our method is a robust and efficient alternative to reproduce shortest-path-like networks. Furthermore, we test resilience to infrastruc-

* alessandro.lonardi@tuebingen.mpg.de

† caterina.debacco@tuebingen.mpg.de

tural failures of the resulting optimal networks. Results show how the geographical locations of stations, and their degree, are decisive factors in efficiently distributing passengers on the metro. Finally, we observe that optimal networks lie in the Pareto front drawn by two fundamental driving forces: the energy dissipated by passengers moving in the network, and the infrastructural cost.

II. RESULTS AND DISCUSSION

A. Multicommodity routing on networks

We design a routing optimization problem on a network $G(V, E)$, where V and E are the sets of nodes and edges, and each edge has length $\ell_e > 0$. The edges are given a conventional orientation stored by a signed incidence matrix, with elements $B_{ve} = \{+1, -1, 0\}$ if e is the head, the tail or neither of them for node v, respectively. We model transportation of $M \geq 1$ commodities through the network, each identified by an index i. We use them to differentiate passengers entering the network from different stations ($i \in V$), so that multiple users sharing the same path catalyze traffic congestion. Suppose that a commodity i has mass S_v^i flowing into node v and outflows S_u^i $\forall u \neq v$, with $\sum_v S_v^i = 0$, $\forall i \in V$, to ensure that the system is isolated.

The main quantities of interest are the edge conductivities $\mu_e \geq 0$, which can be thought of as capacities or, more generally, quantities proportional to the size of the edge. These regulate how passengers flow on the network, as higher conductivity is allocated to edges that are more utilized, while low-conductivity edges are those used by fewer passengers. Hence, determining the values of μ_e, $\forall e \in E$, implies determining the trajectories taken by passengers, and therefore the traffic flow on the network. In our model, the distribution of conductivities is regulated by the following dynamics:

$$\sum_u L_{vu} p_u^i = S_v^i \qquad \forall v \in V, \forall i = 1, \dots, M \quad (1)$$

$$\frac{d\mu_e}{dt} = \mu_e^{\beta-2} f(F_e) - \mu_e \qquad \forall e \in E, \quad (2)$$

where L is the weighted Laplacian matrix of the network, with entries $L_{vu} := \sum_e (\mu_e/\ell_e) B_{ue} B_{ve}$; p_v^i are pressure potentials generated by a commodity i on the nodes; $f(\cdot)$ is a non-negative function of the fluxes F_e, M-dimensional vectors with entries $F_e^i := \mu_e (p_u^i - p_v^i)/\ell_e$, for $e = (u, v)$.

Eq. (1) is Kirchhoff's law, expressing conservation of mass; Eq. (2) regulates the time evolution of the conductivities by means of a feedback mechanism where the higher the flux on an edge, the larger its conductivity μ_e. All commodities share one unique infrastructure, so we follow [25] and assume that μ_e is the same for all i.

The growth in time of μ_e is governed by the function $f(\cdot)$, that in multicommodity optimal transport settings is typically an increasing and differentiable function of some norm of the fluxes [25, 26]. The aim of our work is to investigate how different expressions of $f(\cdot)$ result in different distributions of passengers flows, thus we focus on the following two choices: (i) $f(x) = ||x||_2^2$ (2-norm), and (ii) $f(x) = ||x||_1^2$ (1-norm). The first is supported by theoretical groundings as derived in [25]. However, it may not be the most appropriate one in applications involving transport of passengers, as the 2-norm does not have a straightforward interpretation in these cases. On the contrary, the latter is arguably a more natural choice, backed up by the intuition that edge capacities are controlled by the *number* of passengers traveling on them (instead of the sum of squares). Both norms are taken squared, this is motivated by an analogy between our dynamics and Joule's law in electrical circuits, that we discuss in Section II B.

The contribution of $f(\cdot)$ in the dynamics is balanced by a negative linear contribution in the conductivities, determining their exponential decay in time if no mass is moving through an edge. Note that our dynamics is highly non-linear in μ_e, since solutions of Kirchhoff's law are of the form $p_v^i = \sum_u L_{vu}^\dagger S_u^i$, with $\dagger$ denoting the Moore-Penrose inverse. Finally, the role of the free parameter $0 < \beta < 2$ is to capture different transportation mechanisms: $\beta > 1$ consolidates passengers on fewer edges, following a principle of economy of scale; $\beta < 1$ enforces passengers to distribute more broadly along the network; $\beta = 1$ is shortest-path like.

B. Connection with optimal transport

The dynamics introduced in Section II A has a strong connection with optimal transport theory. In fact, in [25] it is shown that *stationary trajectories* of Eqs. (1) and (2) are also stationary points of the minimization problem:

$$\min_{F \in \mathbb{R}^{|E| \times M}} J := \frac{1}{2} \sum_e \frac{\ell_e}{\mu_e} f(F_e) \quad (3)$$

$$\text{s.t.} \quad \sum_e \ell_e \mu_e^{2-\beta} = K^{2-\beta} \quad (4)$$

$$\sum_e B_{ve} F_e^i = S_v^i \quad \forall v \in V, \forall i = 1, \dots, M, \quad (5)$$

for a fixed constant $K > 0$ and where J is the dissipation cost. Particularly, they both satisfy the scaling $\mu_e \sim f(F_e)^\delta$, $\delta = 1/(3-\beta)$. One can thus rewrite more compactly the previous optimization problem to that of minimizing $J_\Gamma := \sum_e \ell_e f(F_e)^\Gamma$, with $\Gamma = (2-\beta)/(3-\beta)$, generalizing Banavar *et al.* [36].

The crucial distinction between the 1-norm and 2-norm dynamics is that the latter admits the Lyapunov function

$$\mathcal{L}_\beta(\{\mu_e\}) := \frac{1}{2} \sum_{i,v} p_v^i S_v^i + \frac{1}{2(2-\beta)} \sum_e \ell_e \mu_e^{2-\beta}, \quad (6)$$

which enables to prove that *asymptotics* of the dynamics minimize J [25]. Noticeably, the first sum in Eq. (6) is

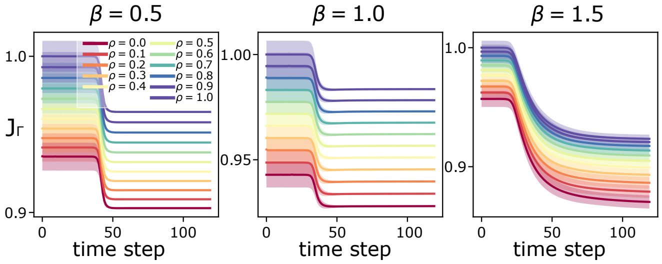

FIG. 1. **Validation of the dynamics with the 1-norm.** We show the dissipation cost evolution along solution trajectories of Eqs. (1) and (2). Results are displayed for different combinations of the parameters ρ and β, and are averaged over 100 runs with random initializations of $\mu_e(0) \sim U(0,1)$. The curves are normalized in $(0,1)$. Shaded areas denote standard deviations, these are thicker for $\beta > 1$ since $\mathcal{L}_\beta$ is concave, with a rich landscape a local minima.

equivalent to $J = \sum_e \ell_e ||F_e||_2^2/\mu_e$ (see Methods IV A), reason for which the 2-norm cost appears to be the most natural formulation of Joule's law.

The second term in Eq. (6) is $W := \left(\sum_e \ell_e \mu_e^\gamma\right)/2\gamma$ with $\gamma = 2 - \beta$, interpretable as the cost to build the network. With this in mind, the Lyapunov functional has the nice interpretation of a sum of dissipation and infrastructural costs.

These theoretical guarantees cannot be easily recovered when we take the 1-norm dynamics. In this case, a Lyapunov functional for Eqs. (1) and (2) is not straightforward to derive. While solving the dynamics may still result in meaningful flows, we cannot guarantee that these solutions minimize the cost J_Γ, i.e. we still have transport but it may not be optimal.

However, we can test this experimentally and we find that (Fig. 1), when applied to the real network of the Paris metro—the main example considered in this work—J_Γ decreases along solution trajectories of the dynamics, with stationary solutions lying in a basin of the cost. Hence, in this case, the conductivities adapt their sizes to reduce energy dissipation. This empirical result is valid for the settings considered in this experiment (and in the remaining of this work), but we observed that this does not apply to, for instance, other smaller synthetic network topologies. Hence practitioners should first validate this behavior in their particular setting. Our validation is performed for several combinations of β and of the input loads $S(\rho)$. The parameter $0 \leq \rho \leq 1$ is progressively smoothing the passengers inflows data collected in [37], with $S(0) = S$ corresponding to the original mass matrix extrapolated from dataset, and $S(1)$ having uniform entries, i.e. the passengers travel with the same rate from each station to all the others (see Methods IV B and IV C for a more detailed explanation).

C. Results on the Paris metro network

In this work, we investigate the applicability of the dynamics in Eqs. (1) and (2) on the Paris metro. Topology data are taken from [38], the network is pre-processed to have a total of $|V| = 302$ nodes and $|E| = 359$ edges, coherently with the observed metro of Paris. As anticipated, we define commodities as stations where passengers enter the network. This means that each vector S^i has only one positive element in $v = i$ (where the passengers of type i enter), while the remaining elements of S^i contain the outflows of passengers who travel from v. Other choices can also be made based on the application, but this will not impact the validity of the model. The values of S^i are fixed using the network manager open data [37] (see Methods IV B for details on data pre-processing and assignation of the users).

We test the two response functions $f(\cdot)$ on this network. Optimal path trajectories resulting in these two cases can be seen in Fig. 2a, where the thickness of each edge is proportional to the fraction of passengers traveling through it. As expected, for $\beta < 1$ optimal transport networks are loopy, with many densely connected edges having fairly uniform fluxes. On the contrary, for $\beta > 1$ optimal topologies are more tree-like, with few central arteries where most of the traffic is concentrated. This applies to both cases.

We notice two distinct behaviors, depending on β. For $\beta < 1$ ($\beta = 0.1$ in Fig. 2a), the solutions cannot be distinguished. This is explained by the Lyapunov functionals $\mathcal{L}_\beta$ being strictly convex in this case, with stationary solutions that correspond to their only minimum. This observation suggests that in the congested transportation regime ($0 < \beta < 1$), where one aims at minimizing traffic congestions, using the theoretically-grounded 2-norm is equivalent to the more intuitive 1-norm formulation. This is not the case for $\beta > 1$, where the two dynamics favor different local minima. These correspond to optimal networks with distinct central arteries where passengers are directed. The differences are further highlighted in Fig. 2b, where the edges are colored with flux differences in these two cases, and where we highlight with markers instances of different stations highly traversed by the two norms. In detail, we can see that two routes branch from Charles de Gaulle-Étoile, the upper one passing by Place de Clichy is favored by the 1-norm, and the lower one reaching Saint-Lazare is preferred by the 2-norm. As for the connection between Châtelet and Gare de Lyon, we observe that the 1-norm tends to favor the shortest path between the two stations, with most of the passengers travelling in a straight line. On the contrary, the path selected by the 2-norm has a deflection.

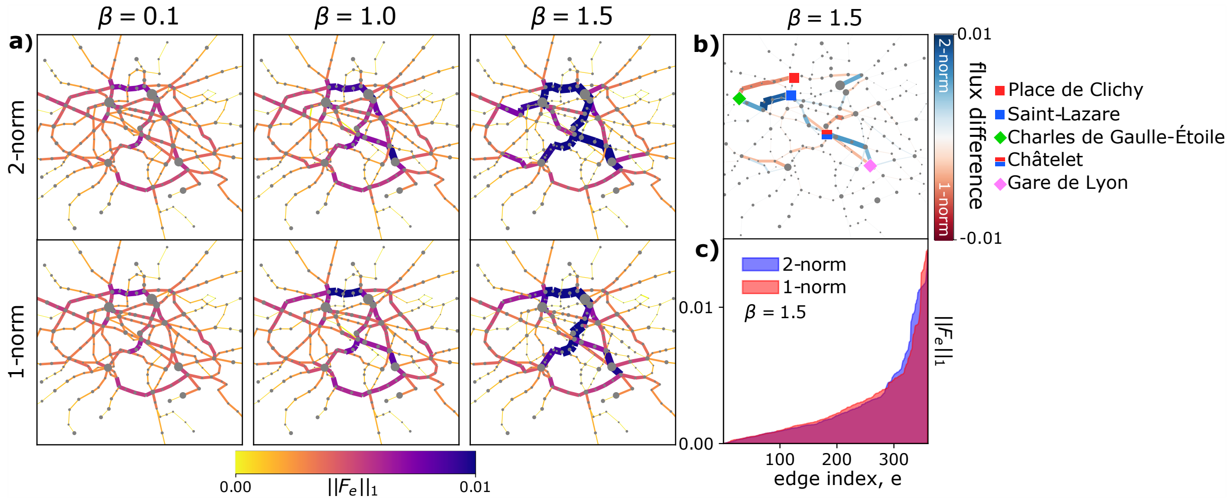

FIG. 2. **Optimal transport networks panel.** **(a)** Optimal transport networks with $\beta = 0.1, 1.0, 1.5$ for the 1-norm and 2-norm response functions. Edge thickness and color are proportional to $||F_e||_1$, normalized to sum to 1; node sizes are proportional to the number of passengers entering them. All the quantities are averaged over 100 runs of the dynamics with $\mu_e(0) \sim U(0,1)$. **(b)** Network colored using the difference of the fluxes obtained with the 1-norm and with the 2-norm. Results are displayed for $\beta = 1.5$, and using the data of Fig. 2a. Widths of edges are proportional to the absolute value of the flux difference, so that by matching the color and size information it is possible to distinguish differences in resulting networks generated by the two response functions. Markerd stations are those discussed in Section II C **(c)** Sorted flux distribution over the edges for $\beta = 1.5$. All quantities have been computed setting the validation forcing parameter $\rho = 0.0$, i.e. $S(\rho = 0.0) = S$ (see Methods IV B and IV C). Similar panels for $\rho = 0.5$ and $\rho = 1.0$ can be found in Supplementary Figs. S1 and S2.

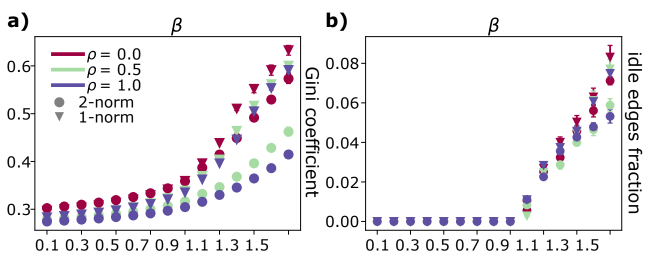

FIG. 3. **Evaluation metrics for the optimal transport networks**. **(a)** Gini coefficient vs. β. **(b)** Idle edges fraction vs. β. Each point is averaged over 100 runs of the dynamics with random initializations of the conductivities, $\mu_e(0) \sim U(0,1)$.

Stimulated by these qualitative differences, we investigate different metrics for an in-depth quantitative evaluation for the case $\beta = 1.5$. First, analyzing the sorted distributions of the fluxes $||F_e||_1$ in Fig. 2c, we notice that the 1-norm dynamics has a more pronounced fat-tailed distribution with a sharper and higher peak. This means that the 1-norm tends to concentrate fluxes on fewer edges. Such effect becomes visibly starker for more homogeneous distributions of passengers entering the stations, i.e. setting $\rho = 0.5, 1.0$ (see Supplementary Figs. S1 and S2).

This can be better quantified by the Gini coefficient [39], which measures the degree of inequality, in this case, of the usage of network edges. It is defined as:

$$\text{Gini coefficient}(x) := \frac{1}{2|E|^2\bar{x}} \sum_{m,n} |x_m - x_n| \qquad (7)$$

for a quantity x, with $\bar{x} = \sum_e x_e/|E|$ being its mean, and m, n denoting edges. In our analysis we set $x_e = ||F_e||_1$. Results are shown in Fig. 3a, where the Gini coefficient is plotted against β for different values of ρ.

As expected, the Gini coefficient increases with β, where paths are more concentrated along fewer edges. The values for the two dynamics are similar for $\beta < 1$, for the reasons mentioned above. Instead, for $\beta > 1$, the markers progressively separate as β increases. The 2-norm has always smaller values than their counterparts, further demonstrating the tendency of the 2-norm to dilute fluxes on a larger area of the network.

We then study the behavior of the fraction of idle edges, i.e. the number of edges with negligible fluxes, divided by the total number of edges $|E|$, see Fig. 3b. This quantity manifests a sudden phase transition at $\beta = 1$, where the dynamics switches from an homogeneous distribution of passengers on the entire network infrastructure, to a distribution progressively more concentrated on a smaller fraction of edges, as β increases. Finally, the 2-norm dynamics returns fewer idle edges than the 1-norm one, as paths are less concentrated.

To summarize, we observe two main findings. First, we noticed that in the regime of $\beta < 1$ the 1-norm and the 2-norm produce identical optimal networks. This result does not hold for $\beta > 1$, in the regime where

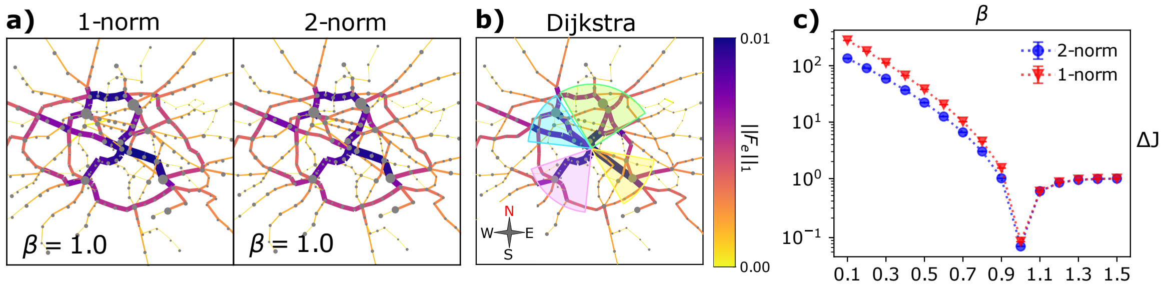

FIG. 4. **Comparison between our methods and Dijkstra's algorithm.** Lenghts of edges are $\tilde{\ell}_e = \ell_e/n_e$, with n_e number of vehicles passing through e as in [38]. This rescaling has been performed following the intuition that metro users moving along the network may travel using the fastest route (that for paths of the same length is the one with more frequent trains) to reach their destination; this may not correspond to the geographically shortest one. **(a)** Optimal transport networks for our methods. Quantities are computed over 100 runs of the dynamics with random initialization of the conductivities, $\mu_e \sim U(0,1)$. **(b)** Optimal transport network computed with Dijkstra's algorithm. For all three networks, edge widths and colors are $||F_e||_1$, and the size of each node is proportional to the number of passengers entering in it. **(c)** Relative energy difference between our methods and Dijkstra's, taken in absolute value. Error bars are standard deviations over 100 realizations.

many local minima in the Lyapunov $\mathcal{L}_\beta$ generate different optimal paths. Second, analyzing the fraction of idle edges, the Gini coefficient of the fluxes, and their distribution, we found that in the regime of branched transportation ($1 < \beta < 2$), the 2-norm tends to limit more traffic congestion, as paths are less consolidated into fewer edges compared to the 1-norm.

D. Comparison with Dijkstra algorithm

As discussed, the main property connecting our 2-norm dynamics with optimal transport is that its stationary solutions are minimizers of the cost $J_\Gamma = \sum_e \ell_e ||F_e||_2^{2\Gamma}$, with $\Gamma = (2-\beta)/(3-\beta)$ [25]. This cost, for $\beta = 1$ and $M = 1$ is equivalent to that of [15, 16] and, as proved by the authors, has optimal fluxes taking the shortest path from their source to their sink. A theoretical generalization of this result to the multicommodity setup is not trivial. In fact, for the 2-norm case the cost reads $J_\Gamma = \sum_e \ell_e \sqrt{\sum_i (F_e^i)^2}$, that is not linear in the commodities, i.e. searching for its minimizer does not correspond to solving M uni-commodity problems, one for each i, and then overlapping them. As for the 1-norm, the dissipation cost with $\beta = 1$ is $J_\Gamma = \sum_e \sum_i \ell_e |F_e^i|$, and therefore its unique global minimum corresponds to that obtained overlapping M shortest paths. However, the 1-norm dynamics is not proved to be equivalent to a gradient flow converging to such minima, thus not providing any theoretical guarantees.

Nevertheless, we can still numerically compare our methods with a shortest path routine using Dijkstra's algorithm [35]. Precisely, we iterate over the commodities and assign a flux F_e^i equal to the fraction of passengers moving from the source v to the sink u, to each edge belonging the shortest path between v and u—the latter computed with Dijkstra's algorithm.

We compare the optimal transport networks obtained using our methods with $\beta = 1$ (Fig. 4a) with the networks returned by Dijkstra's algorithm (Fig. 4b). The three graphs are visibly similar but not identical. Particularly, we focus on the four highlighted areas in Fig. 4b, containing the main branches departing from the central area of the city of Paris. We see that the more trafficked routes in the pink South-West region are identical for our methods and for Dijkstra's one. Traffic in the Nort-West blue region seems to be more diluted for our methods, with the 2-norm optimal network being slightly more similar to Dijkstra's. As for the North green region, both our algorithms concentrate traffic in a curved branch covering a large portion of the Northside of the city. This route is not prioritized in Fig. 4b, as traffic in the green portion is more distributed. Finally, in the South-East yellow area, there is only one main route branching from the city center, while its shape is straight for Dijkstra's, our methods favor a slight deflection.

We attribute these differences in the optimal topologies to the high complexity of the energy landscape of J_Γ. In fact, while Dijkstra's algorithm computes and overlaps each source-sink shortest path separately, our methods treat all the commodities at once. This may lead to convergence in suboptimal points, in particular around $\beta = 1$, where the cost transitions from being strictly convex to strongly concave. While our method in this case may not always reach an optimal solution, it has the practical advantage of being significantly faster than Dijkstra's. Indeed, our algorithms return an optimal solutions in seconds, while Dijkstra's routine implemented in [40] converges in ~ 10 minutes on the Paris metro network.

Lastly, we test the deviation of the cost of our methods from Dijkstra's one. In Fig. 4c we plot the relative cost difference taken in absolute value, that is $\Delta J := |J_\Gamma - J_{\text{Dijkstra}}|/J_{\text{Dijkstra}}$, with Dijkstra's network cost calculated as $J_{\text{Dijkstra}} = \sum_e \ell_e ||F_e||_1$. This has a sharp drop at $\beta = 1$, where traffic is not favored nor penalized, with the

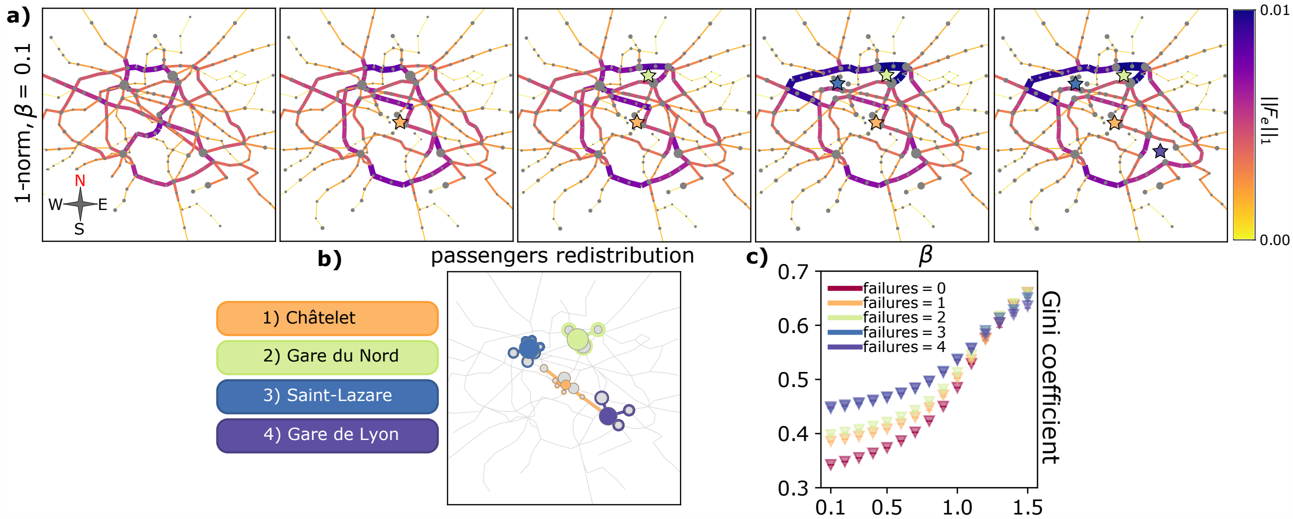

FIG. 5. **Traffic rerouting after network structural failures.** **(a)** We plot the optimal transport networks after nodes trimming. Edge widths and color are $||F_e||_1$, the size of each node is proportional to the number passengers entering it. All quantities are averaged over 100 runs of the dynamics with random initialization of the conductivities, $\mu_e \sim U(0,1)$. Stars highlight the positions of the removed stations, following the same scheme of Fig. 5b. **(b)** Network showing which stations have been removed, these correspond to the fully colored nodes, with colors chosen according to the legend on the left. Colored edges, and nodes with colored borders are those where the passengers get redirected. The colored borders are proportional to the passengers' growth. **(c)** Gini coefficients vs. β, errorbars are standard deviations. Points are colored following the scheme used in the rest of the panel. Similar results for the 2-norm dynamics are in Supplementary Fig. S3.

cost of our network that is similar to the actual shortest path one returned by Dijkstra's algorithm. For $\beta < 1$ we have $J_\Gamma > J_{\text{Dijkstra}}$, showing that penalizing traffic congestion has the drawback of producing more expensive infrastructures. We observe the opposite behavior for $\beta > 1$, where $J_\Gamma < J_{\text{Dijkstra}}$, with congested networks that are progressively cheaper as β increases.

E. Network robustness to failures

Having analyzed how the two dynamics result in networks with different flows of passengers, we now investigate their robustness to structural failures, i.e. removal of nodes. In particular, we study which stations play a central role in alleviating traffic overload in the congested transportation regime. To assess this, we run our dynamics with $\beta = 0.1$, a small value of the critical exponent prone to favor homogeneous distributions of fluxes, and we calculate the Gini coefficient.

In detail, we remove sequentially a total of four stations from the network: Châtelet, Gare du Nord, Saint-Lazare, and Gare de Lyon. The last three are those with the largest number of passengers entering them, while Châtelet has a central position and a high node degree $d = 8$. Once each station was removed, all the passengers that were entering it have been redirected to its neighboring nodes, and then solutions of the dynamics were found with this setting, as depicted in Fig. 5.

In Fig. 5a we display the $1+4$ network obtained removing none, and the stations indicated in Fig. 5b. In Fig. 5c we plot the Gini coefficients of the optimal transport networks against β. Looking at this last plot we notice that for $\beta > 1$ all the points collapse together, regardless of the number of failures. This scenario, however, is of little interest in the situation we want to address, being flux aggregation already favored by $\beta > 1$. As for $\beta < 1$, the difference in Gini coefficient gets wider the lower the β, with the largest difference found at $\beta = 0.1$, we thus investigate this case in more detail.

Removing Châtelet from the network causes a considerable jump in the Gini coefficient. In fact, as we see from the second plot in Fig. 5a, all the passengers who were travelling on the South-West route branching from the city center are redirected, with the consequence of congesting the Southern arteries of the network. Removing Gare du Nord is not as crucial in terms of traffic rerouting. Indeed, the main difference between the second and the third network of Fig. 5a is that those passengers who were departing from Gare du Nord move to its Southern neighbouring station, Gare de l'Est, and modify only slightly their path. A large jump in the Gini coefficient is visible after removing Saint-Lazare, which seems to be crucial in connecting the central part of the city to its Northside. In the fourth plot in Fig. 5a we can see how traffic becomes highly congested in the North branch directed from East to West. Gare de Lyon causes a negligible change in the Gini coefficient, associated with only a modest traffic rerouting visible in the South-East part of the network.

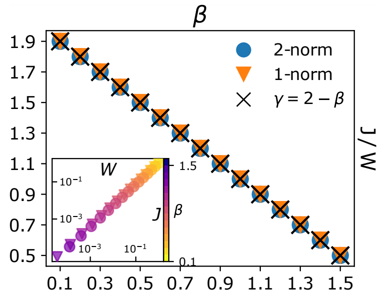

FIG. 6. **Pareto front.** We plot the dissipation/infrastructure cost ratio vs. β. Different points are averaged over 100 runs with random initialization of the conductivities, $\mu_e(0) \sim U(0,1)$. Inset: infrastructure cost, W, vs. dissipation cost, J. Marker shapes are identical to those of the main plot, colors follow the colorbar over β.

F. Pareto front

To conclude our analysis of the multicommodity routing problem it is possible to verify that stationary solutions of Eqs. (1) and (2) lie in the Pareto front (Fig. 6), which can be expressed in closed form as:

$$\frac{J}{W} = \gamma, \tag{8}$$

with $\gamma = 2 - \beta$ (see Methods IV D).

Moreover, looking at the inset of Fig. 6 and Fig. 3 we can observe that the Gini coefficient and the fraction of idle edges can be interpreted as driving forces responsible for the design of the optimal transport network, counterbalancing its cost. In fact, congested transport networks obtained for low values of beta β have a high cost, but are more resilient to damage—low Gini and no idle edges—being their infrastructure densely connected. On the contrary, setting β large has the effect of producing sparse networks. These infrastructures have the benefit of being cheaper, but they are less resistant to node and edge failures, as mentioned in Section II E.

III. CONCLUSIONS

Multicommodity routing is a powerful tool to model optimal network configurations in transportation systems [18]. In this work, we developed a robust and fast model able to perform this task finding stationary solutions of a dynamical system controlling fluxes and conductivities of edges. Our dynamics extends previous works focusing solely on the uni-commodity [15, 27, 28, 30, 41], and on the multicommodity setup [25, 26, 34].

Precisely, we propose two different response functions regulating the growth of conductivities, whose evolution in time is dictated by the passengers moving in the metro infrastructure. We performed a thorough empirical study of the optimal transport networks topologies resulting in the two cases. Using metrics like the fraction of idle edges and the Gini coefficient of the edge fluxes, we found that the two functions behave similarly in the congested transportation regime, but differently in the branched transportation one. In this case, the 1-norm dynamics produces flows that are more concentrated on fewer edges, potentially leading to traffic overload. We addressed the capability of our method to recover shortest path networks by comparing it with Dijkstra's routine. Such comparison showed that our approach is a viable computational alternative to perform this task, achieving accurate results and being scalable for large networks. Additionally, we performed an experiment to measure network robustness to infrastructural failures, revealing that the stations of Châtelet and Saint-Lazare are crucial to ease congestion of metro routes. Finally, we showed that solutions of our model lie in the Pareto front drawn by the energy dissipated during transport and the network infrastructural cost.

Altogether, our findings extend the current research in multicommodity routing problems using optimal transport principles. Our efficient implementation of the method, and the insights provided by the empirical analysis of the network characteristics resulting in the various optimization settings considered here, help to understand the mechanism underlying passenger flows in transportation systems.

Our formalism can be further extended to other possible applications related to the flow of passengers in transport networks. An example could be to incorporate time dependences in the passengers' inflows, thus modeling scenarios where stations are subject to different loads during a day. We would like to remark that our approach is applicable to a variety of practical problems unrelated to transportation systems. A practitioner may then consider response functions for the dynamics alternative to those studied in this work. The analysis performed in this work show how such a problem can be addressed and paves the way for further research beyond urban transportation networks.

IV. METHODS

A. Lyapunov and dissipation cost equivalence

Here we show that the first term of the Lyapunov functional in Eq. (6) is identical to the 2-norm dissipation cost $J = (1/2)\sum_e \ell_e ||F_e||_2^2/\mu_e$, we follow [25]. Multiplying both sides of Eq. (1) for p_v^i and summing over i and v yields the chain of equalities

$$\sum_{i,v,u,e} (\mu_e/\ell_e) B_{ue}\, B_{ve} p_u^i p_v^i = \sum_{i,v} p_v^i S_v^i \tag{9}$$

$$\sum_e \frac{\ell_e}{\mu_e} ||F_e||_2^2 = \sum_{i,v} p_v^i S_v^i, \tag{10}$$

where we made explicit the network Laplacian entries $L_{vu} := \sum_e (\mu_e/\ell_e) B_{ue} B_{ve}$, and we used the definition of the fluxes $F_e^i := \mu_e(p_u^i - p_v^i)/\ell_e$, for $e = (u,v)$, and $\forall i$. Eq. (10) is the identity we wanted to prove.

B. Preprocessing

The original dataset in [38] is provided as a multilayer network embedded with different transportation types, thus we performed a pre-processing to extract the metro network. First, we trimmed nodes belonging to other layers and then merged redundant stations having the same name by collapsing them together. This redundancy was due to the presence of stations with two entrances located in slightly different geographical positions; their coordinates displacement was always negligible compared to the physical extension of the whole network. The trimmed graph reflects consistently the real topology of the Paris metro. For convenience, the longitude and the latitude of nodes are rescaled within the range $[0, 1]$.

We did not have access to the exact travel routes data, so we assigned the entries of S based on the "importance" of each station. In fact the number of users validating their tickets when entering a station, the only data at disposal, is easier to track than the number of exiting users together with their entrance station. In practice, we assigned $N-1$ positive "influence factors" to each station i, one for each node $u \neq i$ where the users entering in i can potentially exit: $r_u^i = g^u / \sum_{w \neq i} g^w$, instead $r_{v=i}^i = 0$, where g^v is the amount of users entering the metro from $v = i$. Note that $0 \leq r_v^i \leq 1$ for all v nodes, and $\sum_{v \neq i} r_v^i = 1$. Thus, we can estimate the number of people exiting from a station $u \neq i$ by assigning $S_u^i = -r_u^i g^{v=i}$, while $S_{v=i}^i = g^v$. The intuition is that a station with a high entering volume of passengers, i.e. high g^v, should have a large amount of exiting users, thus its "influence" value r should be high.

C. Validation

In Section II B we validate Eqs. (1) and (2) with the 1-norm for different configurations of the input forcings. In particular, we define $g^v(\rho) = g^v - \rho(g^v - \langle g \rangle)$ where $\langle g \rangle$ is the average number of passengers entering the stations, and $0 \leq \rho \leq 1$ a parameter. Using the newly defined $g(\rho)$ we build $S(\rho)$ following the "influence assignment" described in Methods IV B. Note that while ρ approaches 1 the passengers tend to distribute uniformly in the network, with the limit case being $\rho = 1$ for which $S_{v=i}^i = \langle g \rangle$, and $S_u^i = -\langle g \rangle / (|V| - 1)$ for all $u \neq v = i$.

D. Pareto front derivation

To obtain the Pareto form in closed form as in Eq. (8) it is sufficient to exploit the scaling $\mu_e \sim (F_e)^\delta$, $\delta = 3 - \beta$, valid for stationary solutions of the multicommodity dynamics. In particular, it is immediate to recover Eq. (8) by rewriting J in Eq. (3) as a function of the conductivities μ_e.

DATA AVAILABILITY

All data used for the experiments on the Paris metro network are publicly available [37, 38].

CODE AVAILABILITY

An open-source implementation of the code is accessible at `https://github.com/aleable/McOpt`.

ACKNOWLEDGMENTS

We thank Enrico Facca for helpful discussions and for insightful comments improving the manuscript. We acknowledge the help of Daniela Leite for data pre-processing. The authors thank the International Max Planck Research School for Intelligent Systems (IMPRS-IS) for supporting Alessandro Lonardi.

[1] K. Sinclair and R. C. Ball, Mechanism for Global Optimization of River Networks from Local Erosion Rules, Phys. Rev. Lett. **76**, 3360 (1996).
[2] A. Rinaldo, I. Rodriguez-Iturbe, R. Rigon, R. L. Bras, E. Ijjasz-Vasquez, and A. Marani, Minimum energy and fractal structures of drainage networks, Water Resources Research **28**, 2183 (1992).
[3] A. Rinaldo, I. Rodriguez-Iturbe, R. Rigon, E. Ijjasz-Vasquez, and R. L. Bras, Self-organized fractal river networks, Phys. Rev. Lett. **70**, 822 (1993).
[4] T. Sun, P. Meakin, and T. Jøssang, Minimum energy dissipation model for river basin geometry, Phys. Rev. E **49**, 4865 (1994).
[5] A. Konkol, J. Schwenk, E. Katifori, and J. B. Shaw, Interplay of river and tidal forcings promotes loops in coastal channel networks (2021), arXiv:2108.04151 [physics.geo-ph].
[6] H. Ronellenfitsch and E. Katifori, Global Optimization, Local Adaptation, and the Role of Growth in Distribution Networks, Phys. Rev. Lett. **117**, 138301 (2016).
[7] H. Ronellenfitsch and E. Katifori, Phenotypes of vascular flow networks, Phys. Rev. Lett. **123**, 248101 (2019).
[8] E. Katifori, G. J. Szöllősi, and M. O. Magnasco, Damage and Fluctuations Induce Loops in Optimal Transport

Networks, Phys. Rev. Lett. **104**, 048704 (2010).

[9] Q. Xia, The formation of a tree leaf, ESAIM: Control, Optimisation and Calculus of Variations **13**, 359 (2007).

[10] A. Tero, S. Takagi, T. Saigusa, K. Ito, D. P. Bebber, M. D. Fricker, K. Yumiki, R. Kobayashi, and T. Nakagaki, Rules for Biologically Inspired Adaptive Network Design, Science **327**, 439 (2010).

[11] A. Tero, K. Yumiki, R. Kobayashi, T. Saigusa, and T. Nakagaki, Flow-network adaptation in Physarum amoebae, Theory in biosciences **127**, 89 (2008).

[12] A. Tero, R. Kobayashi, and T. Nakagaki, Physarum solver: A biologically inspired method of road-network navigation, Physica A: Statistical Mechanics and its Applications **363**, 115 (2006), information and Material Flows in Complex Networks.

[13] A. Tero, R. Kobayashi, and T. Nakagaki, A mathematical model for adaptive transport network in path finding by true slime mold, Journal of Theoretical Biology **244**, 553 (2007).

[14] H. Yamada, A. Toth, and T. Nakagaki, Intelligence: Maze-solving by an amoeboid organism, Nature **407**, 470 (2000).

[15] V. Bonifaci, K. Mehlhorn, and G. Varma, Physarum can compute shortest paths, Journal of Theoretical Biology **309**, 121 (2012).

[16] V. Bonifaci, Physarum can compute shortest paths: A short proof, Information Processing Letters **113**, 4 (2013).

[17] V. Bonifaci, A revised model of fluid transport optimization in Physarum polycephalum, Journal of mathematical biology **74**, 567 (2017).

[18] K. Salimifard and S. Bigharaz, The multicommodity network flow problem: state of the art classification, applications, and solution methods, Operational Research (2020).

[19] C. H. Yeung and D. Saad, Networking - A Statistical Physics Perspective, Journal of Physics A Mathematical and Theoretical **46**, 103001 (2011).

[20] C. H. Yeung, D. Saad, and K. Y. M. Wong, From the physics of interacting polymers to optimizing routes on the London Underground, Proceedings of the National Academy of Sciences **110**, 13717 (2013).

[21] F. Altarelli, A. Braunstein, L. Dall'Asta, C. De Bacco, and S. Franz, The edge-disjoint path problem on random graphs by message-passing, PLOS ONE **10**, 1 (2016).

[22] C. De Bacco, S. Franz, D. Saad, and C. H. Yeung, Shortest node-disjoint paths on random graphs, Journal of Statistical Mechanics: Theory and Experiment **2014**, P07009 (2014).

[23] Y. Xu, H. F. Po, C. H. Yeung, and D. Saad, Scalable Node-Disjoint and Edge-Disjoint Multi-wavelength Routing (2021), arXiv:2107.00609 [physics.soc-ph].

[24] C. H. Yeung and D. Saad, Competition for Shortest Paths on Sparse Graphs, Phys. Rev. Lett. **108**, 208701 (2012).

[25] A. Lonardi, E. Facca, M. Putti, and C. De Bacco, Designing optimal networks for multicommodity transport problem, Phys. Rev. Research **3**, 043010 (2021).

[26] V. Bonifaci, E. Facca, F. Folz, A. Karrenbauer, P. Kolev, K. Mehlhorn, G. Morigi, G. Shahkarami, and Q. Vermande, Physarum Multi-Commodity Flow Dynamics (2021), arXiv:2009.01498 [cs.DS].

[27] E. Facca, F. Cardin, and M. Putti, Towards a Stationary Monge-Kantorovich Dynamics: The Physarum Polycephalum Experience, SIAM Journal on Applied Mathematics **78**, 651 (2016).

[28] E. Facca, S. Daneri, F. Cardin, and M. Putti, Numerical Solution of Monge-Kantorovich Equations via a Dynamic Formulation, Journal of Scientific Computing **82**, 68 (2020).

[29] E. Facca, F. Cardin, and M. Putti, Physarum Dynamics and Optimal Transport for Basis Pursuit (2020), arXiv:1812.11782 [math.NA].

[30] E. Facca, F. Cardin, and M. Putti, Branching structures emerging from a continuous optimal transport model, Journal of Computational Physics **447**, 110700 (2021).

[31] D. Baptista, D. Leite, E. Facca, M. Putti, and C. De Bacco, Network extraction by routing optimization, Scientific Reports **10**, 088702 (2020).

[32] D. Baptista and C. De Bacco, Principled network extraction from images, R. Soc. open sci. **8**, 210025 (2021).

[33] D. Baptista and C. D. Bacco, Convergence properties of optimal transport-based temporal networks (2021), arXiv:2109.00971 [physics.soc-ph].

[34] A. A. Ibrahim, A. Lonardi, and C. De Bacco, Optimal transport in multilayer networks for traffic flow optimization, Algorithms **14**, 10.3390/a14070189 (2021).

[35] E. Dijkstra, A note on two problems in connexion with graphs, Numerische Mathematik **1**, 269 (1959).

[36] J. R. Banavar, F. Colaiori, A. Flammini, A. Maritan, and A. Rinaldo, Topology of the Fittest Transportation Network, Phys. Rev. Lett. **84**, 4745 (2000).

[37] "Trafic annuel entrant par station du réseau ferré 2019", accessed: 2020-08-28 (2019).

[38] R. Kujala, C. Weckström, R. K. Darst, M. N. Mladenović, and J. Saramäki, A collection of public transport network data sets for 25 cities, Scientific data **5**, 180089 (2018).

[39] P. M. Dixon, J. Weiner, T. Mitchell-Olds, and R. Woodley, Bootstrapping the gini coefficient of inequality, Ecology **68**, 1548 (1987).

[40] A. A. Hagberg, D. A. Schult, and P. J. Swart, Exploring Network Structure, Dynamics, and Function using NetworkX, in *Proceedings of the 7th Python in Science Conference*, edited by G. Varoquaux, T. Vaught, and J. Millman (Pasadena, CA USA, 2008) pp. 11 – 15.

[41] D. Hu and D. Cai, Adaptation and Optimization of Biological Transport Networks, Phys. Rev. Lett. **111**, 138701 (2013).

Multicommodity network routing for transportation systems: supplementary information

I. OPTIMAL TRANSPORT NETWORKS

In the following panels we show the optimal transport networks for different configuration of the input forcings $S(\rho)$. In detail, we display the results for $\rho = 0.5$ (Fig. S1), and those for $\rho = 1.0$ (Fig. S2). Looking at the rightmost networks ($\beta = 1.5$) of Fig. S1a and Fig. S2a one can observe a clear tendency of the 1-norm dynamics to concentrate traffic more than the 2-norm one. This trend reflects on the sorted distributions plotted in Fig. S1c and Fig. S2c, where the fluxes are more fat-tailed and homogeneous for the 2-norm. Notably, the effect becomes starker the more the input inflows of passengers distribute uniformly on the nodes, i.e. increasing ρ.

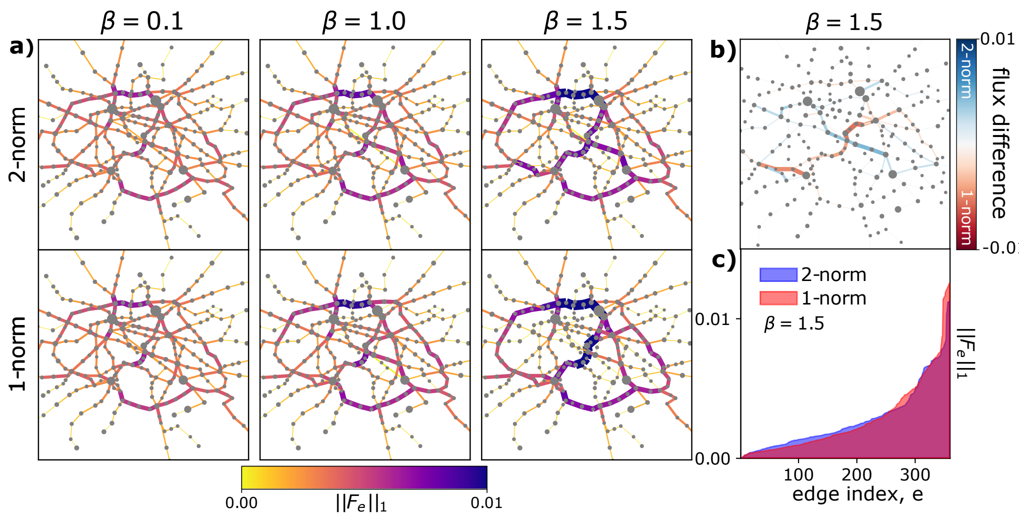

FIG. S1. **Optimal transport networks panel with forcing** $S(\rho = 0.5)$**.** For a detailed description of the subplots one can refer to Fig. 2 in the main text.

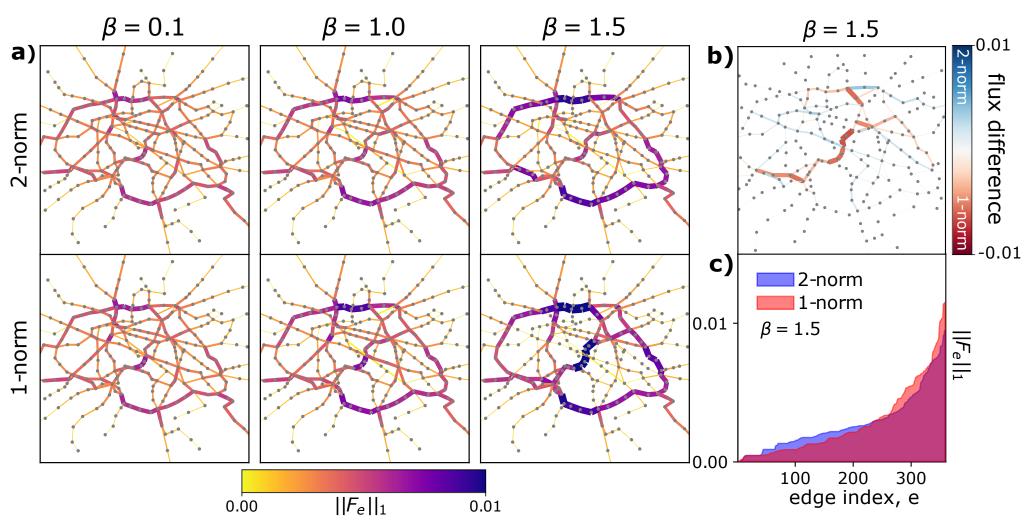

FIG. S2. **Optimal transport networks panel with forcing** $S(\rho = 1.0)$**.** For a detailed description of the subplots one can refer to Fig. 2 in the main text.

II. NETWORK RESISTANCE TO FAILURES: 2-NORM DYNAMICS

In Fig. S3 we reproduce the experiments designed to test the resilience of optimal networks to node failures. Overall, results are similar to those in the main text, it is worth mentioning how the Gini coefficient values Fig. S3c are higher than the correspondent ones for the 1-norm, symptom of the tendency of the latter forcing function to aggregate traffic. Another implication of this effect is that the Gini coefficient values for the 2-norm tend to separate more for higher β than those of the 1-norm. In fact, the latter tend to be overlapped, regardless of the number of failures, on a larger portion of the x-axis (where $\beta > 1$).

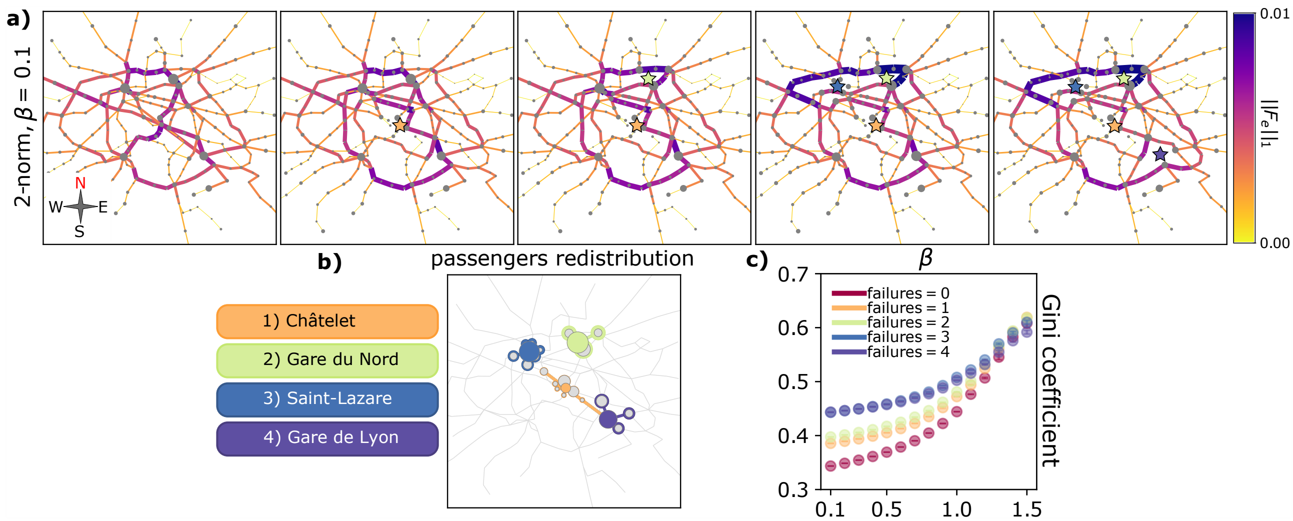

FIG. S3. **Traffic rerouting after network structural failures (2-norm dynamics).** For a detailed description of the subplots one can refer to Fig. 5 in the main text.